

Electronic excitations in semiconductors. II. Application of the theory to diamond

S. Horsch, P. Horsch, and P. Fulde

Max-Planck-Institut für Festkörperforschung, D-7000 Stuttgart 80, Federal Republic of Germany

(Received 27 July 1983)

A previously developed theory for calculating electronic excitations in semiconductors is applied to diamond. The starting point is a self-consistent-field calculation within a given basis set of Gaussian-type orbitals. From that the fully correlated electronic wave function and correlation energy are calculated. The reduction of the direct energy gap and the widths of valence and conduction bands due to correlations are studied and compared with experiments. The results can be understood in terms of simple physical pictures. The largest correlation energy contribution results from the polarization cloud of the excited electron and hole pair, but changes in the ground-state correlations due to the presence of the excited electron are also of importance. Intra-atomic correlations such as relaxation effects are only estimated from molecular calculations. A detailed comparison with other methods is made, in particular with the local approximation to the density-functional formalism.

I. INTRODUCTION

In an earlier paper,¹ denoted in the following by I, a calculation scheme was developed which allows for a quantitative treatment of electron correlations in the excited state of semiconductors. It is based on a previously developed local approach to the correlation problem, which has been tested before for atoms and small molecules.² It also was applied to ground-state calculations of diamond,³ where it was demonstrated that the correlated ground-state wave function of a solid can be calculated with an accuracy which is comparable to that of quantum chemistry calculations for small systems.

The aim of the present investigation is to apply the general theory of electronic excitations in semiconductors to the special case of diamond. There are several reasons for choosing that substance. First of all, there are relatively good self-consistent-field (SCF) calculations available⁴⁻⁶ which are required as a prerequisite for correlation energy calculations. Furthermore, the ground-state wave function and energy have been calculated before as mentioned above. Also, the Wannier orbitals which describe the valence bands are well localized. This facilitates the numerical part of the correlation energy calculations. Finally, it is well known that electronic correlations are very important for an understanding of the excitation spectrum of diamond. For example, SCF calculations yield a direct energy gap which is approximately twice as large as the experimentally observed one, i.e., 15 eV as compared with 7.3 eV.⁷ This difference must then be due to correlations. It is, therefore, of interest to study how the different correlation energy contributions discussed in I result in such a reduction of the gap. Furthermore, the width of the valence bands comes out too large in a SCF calculation, namely 29 eV,⁴ as compared with the experimental value of 24.2 ± 1 eV.⁸ Intuitively, it is obvious that correlations should lead to a reduction of the bandwidth. This is so since the hole (or electron) drags with it a cloud con-

sisting of bond polarizations, relaxed charge distributions, changed ground-state correlations, etc., which make up the quasiparticle.

The present application to diamond of the general theory developed in I is limited to interatomic correlations. They can be described within the space spanned by the bonding and antibonding Wannier functions. This implies that here we can exclude relaxation effects. Their treatment would require working with a larger basis set. This does not pose any problems, but has not been done yet. Their contribution, e.g., to the reduction of the energy gap can be estimated from molecular calculations and is considerably less important than the one due to interatomic correlations. Therefore we will leave a detailed treatment of intra-atomic correlations to a future investigation.

The paper is organized as follows. In Sec. II we list the basic relations which are required for the correlation energy calculations for diamond. Section III is devoted to SCF calculations. They are a prerequisite for correlation energy calculations. In Ref. 3 SCF calculations for diamond were presented. However, while their accuracy was sufficient for ground-state calculations they are not accurate enough for the computation of the SCF energy bands; therefore we improve these calculations by applying a Slater-Koster fit⁹ to the SCF band structure of Mauger and Lannoo.⁴ Section IV contains the interatomic correlation energy calculations for diamond without the changes due to ground-state correlations. The latter are calculated in Sec. V where a discussion of the effect of intra-atomic correlations is also given. These two sections not only give the numerical results for the theory developed in I but also contain their physical interpretation. Although the formalism which is required for a quantitative treatment of the correlation energy is not particularly simple, the final results and the physical picture which emerges from them are simple. Section VI is devoted to a comparison of the present theory with alternative methods. Par-

ticular attention is thereby paid to the local approximation to the density-functional method. Other approaches like the Green's-function method are also discussed. Finally, Sec. VII contains a brief summary and the conclusions.

II. BASIC RELATIONS

We summarize in the following the basic equations which are needed for a correlation energy calculation for diamond. Their derivation as well as further details can be found in I.

The starting point is a basis set of \bar{N} functions $f_i(\vec{r})$ within which all calculations are done. The $f_i(\vec{r})$ consist of groups of Gaussian-type orbitals (GTO's). Their overlap is given by $\langle f_i | f_j \rangle = S_{ij}$. Within the Hilbert space spanned by those functions, the Hamiltonian is written as

$$H = \sum_{i,j,\sigma} \epsilon_{ij} a_{i\sigma}^\dagger a_{j\sigma} + \frac{1}{2} \sum_{\substack{i,j,k,l \\ \sigma,\sigma'}} V_{ijkl} a_{i\sigma}^\dagger a_{k\sigma'}^\dagger a_{l\sigma} a_{j\sigma}. \quad (1)$$

The $a_{i\sigma}$ are the expansion coefficients of the field operators $\Psi_\sigma(\vec{r})$ when expressed in terms of the basis set $f_i(\vec{r})$. The ϵ_{ij} and V_{ijkl} are defined as

$$\epsilon_{ij} = \int d^3r f_i^*(\vec{r}) \left[-\frac{1}{2m} \Delta + V(\vec{r}) \right] f_j(\vec{r}), \quad (2a)$$

$$V_{ijkl} = \int d^3r d^3r' f_i^*(\vec{r}) f_j(\vec{r}) \frac{e^2}{|\vec{r} - \vec{r}'|} f_k^*(\vec{r}') f_l(\vec{r}'). \quad (2b)$$

$V(\vec{r})$ is the single-electron potential and e and m are the electronic charge and mass, respectively. The index i is assumed to contain the cell index \underline{i} of a crystal as well as the index ι describing different functions within the unit cell, i.e., $i = (\underline{i}, \iota)$. The same holds true for the indices j , k , and l .

The SCF ground state of diamond is denoted by $|\Phi_{\text{SCF}}\rangle$. When an electron is added to or taken out of $|\Phi_{\text{SCF}}\rangle$, one obtains the SCF excited states

$$|\Phi_\sigma(\vec{k}, b)\rangle = \begin{cases} c_{\vec{k}b\sigma}^\dagger |\Phi_{\text{SCF}}\rangle, & b = 1, \dots, 4 \\ c_{\vec{k}b\sigma} |\Phi_{\text{SCF}}\rangle, & b = 5, \dots, 8. \end{cases} \quad (3a)$$

$$c_{\vec{k}b\sigma} |\Phi_{\text{SCF}}\rangle, \quad b = 5, \dots, 8. \quad (3b)$$

The operator $c_{\vec{k}b\sigma}^\dagger$ creates an electron with momentum \vec{k} in the conduction band $b = 1, \dots, 4$, while $c_{\vec{k}b\sigma}$ destroys an electron in the valence band $b = 5, \dots, 8$.

In the following we shall consider the case (3a) where an electron is added. All the following equations can be easily changed to the case where an electron is destroyed. The *correlated* wave function is written as

$$|\Psi_\sigma(\vec{k}, b)\rangle = e^S c_{\vec{k}b\sigma}^\dagger |\Phi_{\text{SCF}}\rangle. \quad (4)$$

The operator S is of the form

$$S = - \sum_{m,n} [\eta_{mn}^{(0)} O_{mn} P_{mn}(\vec{k}, b) + \eta_{mn}^{(e)} O_{mn} Q_{mn}(\vec{k}, b)]. \quad (5)$$

The O_{mn} are local operators which generate a correlation hole around each electron. We want to consider only that part of $O_{mn} |\Phi_{\text{SCF}}\rangle$ which generates two-particle excitations out of the ground state. This is done by forbidding any contractions within the O_{mn} operators when expectation values are evaluated. The O_{mn} operators take the following three forms:

$$O_{mn} = \begin{cases} n_{m\uparrow} n_{m\downarrow} \delta_{mn} \\ n_m n_n \left[= \sum_\sigma n_{m\sigma} \sum_{\sigma'} n_{n\sigma'} \right] \\ \vec{s}_m \cdot \vec{s}_n. \end{cases} \quad (6)$$

Furthermore $n_{m\sigma} = b_{m\sigma}^\dagger b_{m\sigma}$ and $(\vec{s}_m)_{\sigma\sigma'} = b_{m\sigma}^\dagger \vec{s}_{\sigma\sigma'} b_{m\sigma}$.

The indices m (and n) refer to local regions which are characterized by local functions $g_m(\vec{r})$. The $b_{m\sigma}^\dagger$ create an electron in state $g_m(\vec{r})$. Again $m = (\underline{m}, \mu)$ consists of a cell index \underline{m} and an index μ for different functions within a cell. The $g_m(\vec{r})$ are expressed in terms of the $f_i(\vec{r})$ as

$$g_m(\vec{r}) = \sum_{i=1}^{\bar{N}} \gamma_{mi} f_i(\vec{r}) \quad (7)$$

and are specified by the matrix γ_{mi} .

The operators $P_{mn}(\vec{k}, b)$ and $Q_{mn}(\vec{k}, b)$ have the properties of projection operators. They are defined by

$$O_{mn} P_{mn}(\vec{k}, b) c_{\vec{k}b\sigma}^\dagger |\Phi_{\text{SCF}}\rangle = c_{\vec{k}b\sigma}^\dagger O_{mn} |\Phi_{\text{SCF}}\rangle, \quad (8)$$

$$O_{mn} Q_{mn}(\vec{k}, b) |\Phi_{\text{SCF}}\rangle = 0.$$

The parameters $\eta_{mn}^{(0)}$ are determined by ground-state calculations. The parameters $\eta_{mn}^{(e)}$ do not follow from a ground-state calculation and are characteristic for the added electron. They are obtained from minimizing the quasiparticle energy $\epsilon(\vec{k}, b)$. The latter is calculated with the help of a linked cluster expansion

$$\epsilon(\vec{k}, b) = \frac{\langle c_{\vec{k}b\sigma} (e^S)^\dagger H e^S c_{\vec{k}b\sigma}^\dagger \rangle_c}{\langle c_{\vec{k}b\sigma} (e^S)^\dagger e^S c_{\vec{k}b\sigma}^\dagger \rangle_c}. \quad (9)$$

Here the subscript c indicates that only connected contractions must be taken when the expectation value is evaluated. The notation $\langle \rangle$ is an abbreviation for $\langle \Phi_{\text{SCF}} | \dots | \Phi_{\text{SCF}} \rangle$. The determining equations for the $\eta_{mn}^{(e)}$ are then

$$\frac{\partial \epsilon(\vec{k}, b)}{\partial \eta_{mn}^{(e)}} = 0. \quad (10)$$

One can decompose $\epsilon(\vec{k}, b)$ into a SCF part $\epsilon_{\text{SCF}}(\vec{k}, b) = \langle c_{\vec{k}b\sigma} H c_{\vec{k}b\sigma}^\dagger \rangle - \langle H \rangle$ and a correlation energy part $\epsilon_{\text{corr}}(\vec{k}, b)$, i.e.,

$$\epsilon(\vec{k}, b) = \epsilon_{\text{SCF}}(\vec{k}, b) + \epsilon_{\text{corr}}(\vec{k}, b). \quad (11)$$

We proceed by showing first how the $\eta_{nm}^{(e)}$ are determined in practice and how $\epsilon_{\text{corr}}(\vec{k}, b)$ is evaluated. This implies the evaluation of the expectation value [Eq. (9)] for diamond, which is the central problem of this paper. Thereby, one replaces $\exp S = 1 + S$. The further evaluation is

done in several steps.

First, one expresses the Bloch states in terms of Wannier functions $w_{t\sigma}^\dagger$, i.e., the corresponding operators are related by

$$c_{\vec{k}b\sigma}^\dagger = N_c^{-1/2} \sum_t e_{\tau}(\vec{k}, b) w_{t\sigma}^\dagger \exp(i\vec{k} \cdot \vec{R}_t). \quad (12)$$

Here, $t = (\underline{t}, \tau)$, and \vec{R}_t denotes the position of the t th unit cell and N_c their number.

Then, the evaluation of Eq. (11) is reduced to the computation of local expectation values

$$\begin{aligned} & \langle w_{t'\sigma} H O_{mn}^{(\kappa)} w_{t\sigma}^\dagger \rangle_c, \\ & \langle w_{t'\sigma} (O_{m'n'}^{(\kappa')})^\dagger H O_{mn}^{(\kappa)} w_{t\sigma}^\dagger \rangle_c, \\ & \langle w_{t'\sigma} (O_{m'n'}^{(\kappa')})^\dagger O_{mn}^{(\kappa)} w_{t\sigma}^\dagger \rangle_c, \end{aligned} \quad (13)$$

where the abbreviations $O_{mn}^{(0)} = O_{mn} P_{mn}$ and $O_{mn}^{(e)} = O_{mn} Q_{mn}$ have been introduced. As it is shown in I, the evaluation of these local matrix elements can be reduced

$$\eta_{mn}^{(e)}(\vec{k}, b) = \sum_{m', n'} \left[(H O_{m'n'}^{(e)})_{\vec{k}b} - \sum_{m'', n''} \eta_{m''n''}^{(0)} ((O_{m''n''}^{(0)})^\dagger [H - \epsilon(\vec{k}, b)] O_{m'n'}^{(e)})_{\vec{k}b} \right] \{ ((O_{i'j'}^{(e)})^\dagger [H - \epsilon(\vec{k}, b)] O_{ij}^{(e)})_{\vec{k}b} \}^{-1}_{m'n'; mn}. \quad (17)$$

The last factor denotes a matrix inversion. Since on the right-hand side (rhs) of that equation $\epsilon(\vec{k}, b)$ appears, which depends on $\eta_{mn}^{(e)}(\vec{k}, b)$ itself, Eq. (17) must be solved self-consistently.

The physical meaning of the different terms entering that equation is the following. The first term on the rhs defines the gain of interaction energy between the charge of the quasiparticle and its polarization cloud as compared to the unpolarized system. The second term containing the ground-state parameters $\eta_{mn}^{(0)}$ introduces the effect of the ground-state correlations on the polarizability of the system. The polarization of the medium is due to particle-hole excitations, their energy together with the dipole-dipole interaction energy enters the denominator of Eq. (17). The parameters $\eta_{mn}^{(e)}$ are determined by the balance of the energy in the numerator and denominator.

After one has determined the $\eta_{mn}^{(e)}(\vec{k}, b)$ the correlation energy can be evaluated according to

$$\begin{aligned} \epsilon_{\text{corr}}(\vec{k}, b) &= \epsilon_{\text{corr}}^{(0)}(\vec{k}, b) + \epsilon_{\text{corr}}^{(e)}(\vec{k}, b), \\ \epsilon_{\text{corr}}^{(0)}(\vec{k}, b) &= - \sum_{m, n} \eta_{mn}^{(0)} (H O_{mn}^{(0)})_{\vec{k}b} \\ &+ \frac{D}{2} \sum_{mn} \frac{\partial \epsilon_{\text{corr}}(\vec{k}, b)}{\partial \eta_{mn}^{(0)}} \eta_{mn}^{(0)}, \\ \epsilon_{\text{corr}}^{(e)}(\vec{k}, b) &= - \sum_{m, n} \eta_{mn}^{(e)} (H O_{mn}^{(e)})_{\vec{k}b}, \end{aligned} \quad (18)$$

with

$$D = 1 + \sum_{m, n, \kappa} \sum_{m', n', \kappa'} \eta_{mn}^{(\kappa)}(\vec{k}, b) \eta_{m'n'}^{(\kappa')}(\vec{k}, b) (O_{m'n'}^{(\kappa')} O_{mn}^{(\kappa)})_{\vec{k}b}. \quad (19)$$

to multiplications of matrices of the form

$$\begin{aligned} R_{im} &= \langle a_{i\sigma}^\dagger b_{m\sigma} \rangle, \quad D_{im} = \langle a_{i\sigma} b_{m\sigma}^\dagger \rangle, \\ \bar{P}_{mn} &= \langle b_{m\sigma}^\dagger b_{n\sigma} \rangle, \quad \bar{D}_{mn} = \langle b_{m\sigma} b_{n\sigma}^\dagger \rangle, \\ C_{it} &= \langle a_{i\sigma} w_{t\sigma}^\dagger \rangle, \quad \bar{C}_{mt} = \langle b_{m\sigma} w_{t\sigma}^\dagger \rangle, \end{aligned} \quad (14)$$

together with the Fock matrix and the interaction matrix V_{ijkl} . Having evaluated these matrices and from them the above local expectation values, one introduces the function

$$G_{it'}(\vec{k}, b) = e_{\tau}^*(\vec{k}, b) e_{\tau}(\vec{k}, b) \exp[i\vec{k} \cdot (\vec{R}_{t'} - \vec{R}_t)]. \quad (15)$$

With its help, one can convert for any operator A the local matrix elements $\langle w_{t'\sigma} A w_{t\sigma}^\dagger \rangle_c$ into the Bloch basis through

$$(A)_{\vec{k}b} = N_c^{-1} \sum_{t, t'} G_{it'}(\vec{k}, b) \langle w_{t'\sigma} A w_{t\sigma}^\dagger \rangle_c. \quad (16)$$

Within that notation the determining Eq. (9) for the parameters $\eta_{mn}^{(e)}(\vec{k}, b)$ leads to (see I)

In the next sections this computational scheme will be applied to diamond and we will follow, thereby, the described procedure step by step.

III. BASIS SET AND WANNIER FUNCTIONS

In this section we describe the construction of the Wannier functions which are required for the correlation energy calculations. SCF calculations for diamond were presented in connection with the ground-state calculations.³

The bonding Wannier functions are closely related to bonding functions $\phi_i(\vec{r})$ which span the space of occupied SCF orbitals in the ground state of diamond and have been calculated in Ref. 3. We first recall the construction of the $\phi_i(\vec{r})$. It is based on a method developed by Stoll and Preuss,^{10,11} which uses localization potentials and applies to closed-shell systems. For the details of the method we refer to the original literature. The calculations of the $\phi_i(\vec{r})$ employ for each atom a $7s/3p$ GTO basis set in a form optimized by Ross and Siegbahn for an isolated C atom. This set is contracted into a set $4s/2p$ with a contraction $4 + 1 + 1/2 + 1$ and contraction coefficients taken from Ref. 12. The normalized Gaussian groups $\psi_1(\vec{r}), \dots, \psi_6(\vec{r})$ are listed explicitly in Table I of Ref. 3. Here these functions are denoted by $f_n(\vec{r})$, where $n = (\underline{n}, \nu)$ consists of a cell index \underline{n} and an index ν counting the basis functions per cell.¹³ Per atom there are 12 basis functions, since each of the p -type Gaussian groups $\psi_5(\vec{r})$ and $\psi_6(\vec{r})$ contains four nonorthogonal functions of p symmetry pointing into the four different bond directions. The occupied SCF orbitals in the ground state are given by

$$\phi_i(\vec{r}) = \sum_n \hat{c}_{in} f_n(\vec{r}), \quad (20)$$

where the \hat{c}_{in} can be found in Table II of Ref. 3. For a given cell i the intracell index $\iota = 1, \dots, 6$, since there are two 1s-core functions and four bonds per cell. The prime in the sum over n implies that only one site contributes to a 1s-core orbital, while for a given bond orbital only those two sites contribute which are adjacent to the bond.

At this point it is advantageous to define from the bond functions $\phi_i(\vec{r})$ atomic hybrid functions $\tilde{f}_n(\vec{r})$ which contain only functions $f_n(\vec{r})$ centered at one particular atom. After they have been orthogonalized to the 1s-core function of the same atom and normalized, the $\tilde{f}_{n\sigma}(\vec{r})$ are given by

$$\tilde{f}_n(\vec{r}) = \sum_{\iota} c_{ni} f_{\iota}(\vec{r}), \quad (21)$$

where the c_{ni} follow from the \hat{c}_{in} of Eq. (20). The nonorthogonal $\tilde{f}_n(\vec{r})$ can be considered as a minimal basis set for the valence electrons, which will be used later when the interatomic correlations are treated. Next we construct from the hybrid functions $\tilde{f}_n(\vec{r})$ bonding and antibonding functions $B_n(\vec{r})$ and $A_n(\vec{r})$,

$$\begin{aligned} B_n(\vec{r}) &= (2 + \tilde{S}_{n\bar{n}})^{-1/2} [\tilde{f}_n(\vec{r}) + \tilde{f}_{\bar{n}}(\vec{r})], \\ A_n(\vec{r}) &= (2 - \tilde{S}_{n\bar{n}})^{-1/2} [\tilde{f}_n(\vec{r}) - \tilde{f}_{\bar{n}}(\vec{r})], \end{aligned} \quad (22)$$

where n and \bar{n} denote the two hybrids out of which the bond n is formed and $\tilde{S}_{n\bar{n}} = \langle \tilde{f}_n | \tilde{f}_{\bar{n}} \rangle$ is the overlap between these orbitals. The core orbitals can already be considered as Wannier functions since their overlap is negligible. The functions $B_i(\vec{r})$ and $A_i(\vec{r})$ must be orthogonalized in two further steps. Firstly, they are orthogonalized with respect to all core states. The resulting bonding functions (labeled by a prime) are then orthogonalized with respect to each other according to

$$\bar{B}_i(\vec{r}) = \sum_j (U^{-1/2})_{ij} B'_j(\vec{r}), \quad (23)$$

with $U_{ij} = \langle B'_i | B'_j \rangle$. For the computation of $U^{-1/2}$ we employed an iteration procedure which is an extension of a technique due to Löwdin.¹⁴ The iteration equation

$$(U^{-1/2})_{n+1} = \frac{1}{2} [3\mathbb{1} - (U^{-1/2})_n U (U^{-1/2})_n] (U^{-1/2})_n, \quad (24)$$

with $(U^{-1/2})_0 = \lambda\mathbb{1}$, has been solved for a cluster of 79 unit cells leading to a high accuracy for $(U^{-1/2})_{ij}$, i.e., the

relative error is less than 10^{-5} . Rapid convergency is obtained for $\lambda = 0.7$. The same procedure is repeated for the antibonding functions $A'_i(\vec{r})$. They are first orthogonalized with respect to the $\bar{B}_i(\vec{r})$ and then with respect to each other.

The completely orthogonalized bonding and antibonding functions $\bar{B}_i(\vec{r})$ and $\bar{A}_i(\vec{r})$ do not yet have the properties of Wannier orbitals as $\langle \bar{A}_i | H_0 | \bar{B}_i \rangle \neq 0$ in distinction to true Wannier functions. A further rotation is required in the space spanned by the $\bar{B}_i(\vec{r})$ and $\bar{A}_i(\vec{r})$ in order to find the true Wannier functions. This is achieved by perturbation theory and resembles therefore, the extended bond orbital approximation (EBOA).¹⁵ The Wannier functions $B_i^E(\vec{r})$ and $A_i^E(\vec{r})$ which block diagonalize the Hamiltonian are

$$B_i^E(\vec{r}) = \left[1 + \sum_j \frac{F_{ij}^2}{\delta^2} \right]^{-1/2} \left[\bar{B}_i(\vec{r}) + \sum_j \frac{F_{ij}}{\delta} \bar{A}_j(\vec{r}) \right], \quad (25)$$

and a similar expression holds for the $A_i^E(\vec{r})$.

Here

$$\delta = \langle \bar{A}_i | H_0 | \bar{A}_i \rangle - \langle \bar{B}_i | H_0 | \bar{B}_i \rangle, \quad F_{ij} = \langle \bar{A}_i | H_0 | \bar{B}_j \rangle$$

are the coupling matrix elements, and H_0 is the SCF part of the Hamiltonian. Instead of calculating δ and the F_{ij} from the functions $\bar{A}_i(\vec{r})$ and $\bar{B}_i(\vec{r})$, we determine them by means of a Slater-Koster representation⁹ of the SCF energy bands of Mauger and Lannoo.⁴ This compensates for the relatively small set of basis functions used in Ref. 3. The point is that the functions $\phi_i(\vec{r})$, as determined by the method of Stoll and Preuss, are slightly too localized as compared to Ref. 4, where a basis of Slater functions has been used. The SCF bands of Mauger and Lannoo are more accurate and have also been used in other investigations.¹⁶ But it should be pointed out that even these bands contain overall uncertainties of about 1 eV.

The Slater-Koster fit has been done for the principal directions $\Delta = [100]$ and $\Lambda = [111]$, where one can make use of symmetry considerations. Thereby the coupling matrix elements F_{ij} are taken into account up to second-nearest neighbors (Table I). The vectors $\vec{R}_n = (a/4)(n_x, n_y, n_z)$ denote the lattice vectors between different bonds i and j , and a is the lattice constant. The energy eigenvalues $\epsilon_{\text{SCF}}(\vec{k}, b)$ which result from the

TABLE I. Parameters of the Slater-Koster representation of the Hartree-Fock (HF) band structure of Mauger and Lannoo. The columns from left to right are the bond coordinates in units of $a/4$, the number of equivalent bonds N_b , the matrix elements between bonding and antibonding functions, respectively, up to third-nearest-neighbor bonds, and the coupling matrix elements between bonding and antibonding functions up to second-nearest neighbors in units of eV.

$\underline{n} = (n_x, n_y, n_z)$	N_b	$\langle \bar{B}_{i\sigma} H \bar{B}_{i+\underline{n},\sigma} \rangle$	$\langle \bar{A}_i H \bar{A}_{i+\underline{n},\sigma} \rangle$	$\langle \bar{B}_{i\sigma} H \bar{A}_{i+\underline{n},\sigma} \rangle$
ξ_0	(0,0,0)	1	-10.10	21.85
ξ_1	(1,1,0)	6	-2.80	-0.55
ξ_2	(2,2,0)	6	0.68	-1.00
ξ_3	(2,1,-1)	12	-0.22	1.25
ξ_4	(2,-2,0)	6	0.02	0.29
ξ_5	(3,-1,0)	12	0.05	-0.36
ξ_6	(3,2,1)	24	-0.15	0.04
ξ_7	(3,3,0)	6	-0.30	0.04

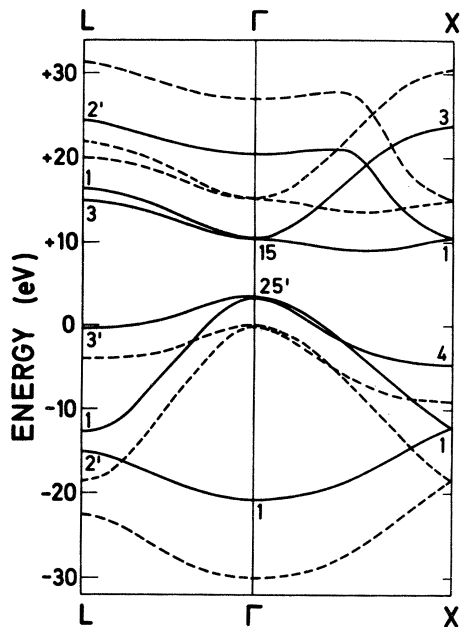


FIG. 1. HF band structure of diamond (dashed lines) obtained by a Slater-Koster representation of the data of Ref. 4. In comparison, the bands (solid lines) are given as obtained within the framework of the present paper, when only polarization effects are taken into account [LA(1) approximation].

Slater-Koster representation are shown in Fig. 1.

Finally we want to mention that the one-particle density matrix shows some deviations when it is calculated with the functions $\bar{B}_i(\vec{r})$ or $B_i^E(\vec{r})$. The changes occur for those matrix elements which refer to second-nearest neighbors where they can be up to 20%. However, at these distances the density matrix elements are already very small for a strongly localized system such as diamond.

IV. INTERATOMIC CORRELATIONS

Interatomic correlations are the dominant electron correlations in covalent semiconductors as far as their contributions to the quasiparticle energy bands are concerned. This is due to the fact that the dielectric response is mainly determined by the polarization of the bonds, which is an interatomic correlation effect. The microscopic correlation energy calculations can, of course, only be performed within a finite cluster around the quasiparticle which is moving with it through the crystal. We shall consider in the following a cluster consisting of a central bond and up to second-nearest-neighbor bonds, Fig. 2. This implies a total of 25 bonds or 130 basis functions $f_n(\vec{r})$. In order to calculate the correlation energy which results from regions outside the cluster, a continuum approximation can be made as will be shown in detail. This section concludes with a discussion of the numerical results obtained for the bands.

The appropriate choice for the functions $g_m(\vec{r})$ [see Eq. (7)] which define the O_{mn} [Eq. (6)] in the case of interatomic correlations are atomic hybrid functions as small-

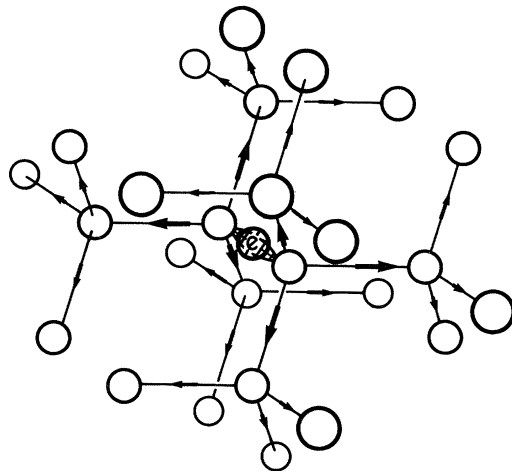


FIG. 2. Cluster containing 25 bonds used for the microscopic calculations of the correlation energy. The arrows indicate the size of the polarization of the bonds around an extra electron located in the central bond of the cluster.

est entities. Here we introduce a set of orthogonal $g_m(\vec{r})$ constructed from the orthogonal functions (23), $\bar{B}_m(\vec{r})$ and $\bar{A}_m(\vec{r})$, according to

$$g_m(\vec{r}) = 2^{-1/2} [\bar{B}_m(\vec{r}) \pm \bar{A}_m(\vec{r})]. \quad (26)$$

Making use of Eqs. (21)–(23), the matrix γ_{mi} in Eq. (7) defining the $g_m(\vec{r})$ in terms of the original basis $f_i(\vec{r})$ can be determined. Constructing the $g_m(\vec{r})$ according to (26) instead from, e.g., the nonorthogonal basis (22) avoids projecting twice out of overlap regions when the correlation operators O_{mn} are applied. In the following we shall consider only density operators O_{mn} [Eq. (6)] and neglect spin-spin correlations since they play a minor role in covalent semiconductors.³ For the numerical calculations it is advantageous to formulate the Hamiltonian also in terms of hybrid functions in order to reduce the number of matrix elements V_{ijkl} . Here, the nonorthogonal set $\tilde{f}_n(\vec{r})$ (21) is better suited than the $g_m(\vec{r})$, since the latter have orthogonalization tails which would imply significantly larger computation times for the V_{ijkl} . All quantities in the Hamiltonian (1) will be denoted by a tilde, i.e., $\tilde{\epsilon}_{ij}$, \tilde{V}_{ijkl} , \tilde{S}_{ij} , etc., and operators $\tilde{a}_{i\sigma}^\dagger$ and $\tilde{a}_{i\sigma}$ replace the $a_{i\sigma}^\dagger$ and $a_{i\sigma}$, respectively. For example,

$$\tilde{V}_{ijkl} = \int d^3r d^3r' \tilde{f}_i^*(\vec{r}) \tilde{f}_j(\vec{r}) \frac{e^2}{|r-r'|} \tilde{f}_k^*(\vec{r}') \tilde{f}_l(\vec{r}'). \quad (27)$$

The dimension of the V_{ijkl} matrix is reduced for the cluster containing 50 hybrids from 130^2 to 50^2 . The computational effort is further reduced considerably by taking into account the symmetry properties of the \tilde{V}_{ijkl} . Within the cluster all four center matrix elements are taken into account except exchange integrals connecting hybrid functions, which are further separated than are second-nearest-neighbor bonds. A careful analysis has shown

that this approximation has negligible effect on the correlation energy. The evaluation of the various density matrices defined by Eqs. (14) and required for the computation of the expectation values (13) is outlined in Appendix A.

We are now in the position to determine the variational parameters $\eta_{mn}^{(e)}(\vec{k}, b)$ according to Eq. (17) within the cluster defined above. As is seen from Fig. 3, there are 14 different $\eta_{mn}^{(e)}$ parameters for given values of \vec{k} and b which describe density correlations. We shall first neglect the influence of the ground-state correlations on the $\eta_{mn}^{(e)}$, implying that we set $\eta_{mn}^{(0)}=0$ in Eq. (17). Their influence will be discussed in the next section; therefore, the following set of equations must be solved self-consistently

$$\eta_{mn}^{(e)}(\vec{k}, b) = \sum_{m', n'} (HO_{m'n'}^{(e)})_{\vec{k}b} \{ ((O_{ij}^{(e)})_{\vec{k}b})^\dagger [H - \epsilon(\vec{k}, b)] \times O_{ij}^{(e)} \}_{m'n'; mn}^{-1}, \quad (28)$$

together with Eq. (18).

It has been pointed out before that the parameters $\eta_{mn}^{(e)}$ refer to a cluster of 25 bonds called C_2 . However, in diamond roughly $\frac{1}{3}$ of the correlation energy comes from contributions from outside that cluster. They must be incorporated in $\epsilon(\vec{k}, b)$ and therefore in the solution of Eq. (28). Therefore we shall now discuss their inclusion.

For the contributions to the correlation energy coming from outside C_2 we adopt a continuum approximation. Thereby we make use of the fact that for large distances R the field energy of the additional electron in the dielectric medium is proportional to R^{-4} . This implies that the

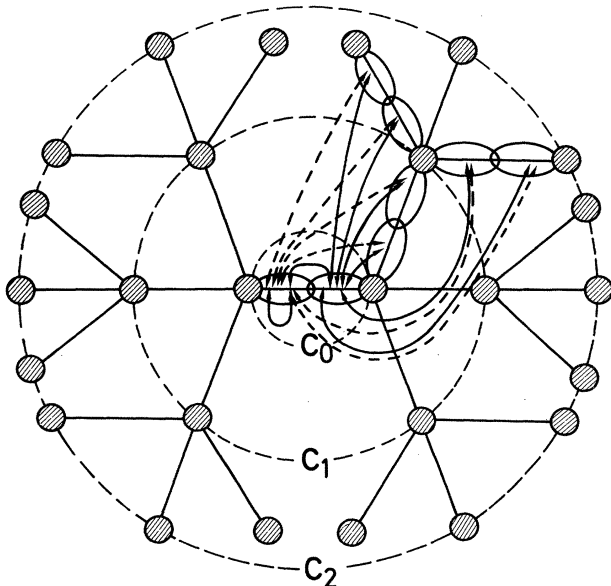


FIG. 3. Schematic view of the cluster C_2 containing 25 bonds. The smaller clusters C_0 and C_1 containing one and seven bonds, respectively, are required for the estimate of the energy contribution from outside the cluster C_2 . The 14 density-density operators O_{mn} connecting different hybrids as defined in Eq. (6) are indicated by arrows.

corresponding correlation energy contributions outside a cluster of radius R should be proportional to R^{-1} . In order to find the proportionality constant we divide the correlation energy contributions from inside the cluster C_2 into two parts:

$$\epsilon_{\text{corr}}(\vec{k}, b; C_2) = \epsilon_{\text{corr}}(\vec{k}, b; C_n) + \delta\epsilon_{\text{corr}}(\vec{k}, b; C_n), \quad (29)$$

Here $\epsilon_{\text{corr}}(\vec{k}, b; C_n)$ is the correlation energy contribution from inside the cluster C_n , which is smaller than C_2 and given either by C_0 (central bond) or C_1 (central bond plus nearest neighbors) (see Fig. 3). The total correlation energy including the contributions from outside the cluster C_2 is then obtained by scaling the energy $\delta\epsilon_{\text{corr}}(\vec{k}, b; C_n)$ of the shell formed by the two clusters C_n and C_2 :

$$\epsilon_{\text{corr}}^{(n)}(\vec{k}, b) = \epsilon_{\text{corr}}(\vec{k}, b; C_2) + S_n \delta\epsilon_{\text{corr}}(\vec{k}, b; C_n). \quad (30)$$

The scaling factor $S_n = R_n^{1/3}/(1 - R_n^{1/3})$ is defined in terms of the volume ratio $R_n = V(C_n)/V(C_2)$ of the two clusters C_n and C_2 . The volume ratio is determined by the numbers of bonds within the clusters; hence no additional parameters appear. For C_0 it is $R_0 = \frac{1}{25}$ and $S_0 = 0.520$, while for C_1 one finds $R_1 = \frac{7}{25}$ and $S_1 = 1.892$. While the scaling becomes exact for large clusters, the quality of the procedure for small clusters can be tested by calculating $\epsilon_{\text{corr}}^{(n)}(\vec{k}, b)$ first with C_0 and then with C_1 and comparing the results for $\epsilon^{(n)}(\vec{k}, b)$ in both cases. We list in Table II the energy differences for four selected points within the Brillouin zone. It is seen that the results vary only by approximately 0.1–0.2 eV when C_0 and C_1 are used. This indicates that the cluster C_2 is sufficiently large in order to yield a reliable extrapolation to infinite range. Note that local field effects are also included outside the cluster C_2 because of the chosen extrapolation procedure and the fact that they are contained in the contribution resulting from inside C_2 . The results for the band structure are shown in Fig. 1. They are obtained by solving Eqs. (28) and (18), and using Eq. (30) with $C_n = C_1$.

As pointed out before, the band-structure results contain the polarization effects but not the changes in the ground-state correlations nor relaxation effects. The main features of the correlated bands as compared with those of

TABLE II. Test of the continuum approximation for selected excitation energies. The first two columns are the SCF excitation energies and the excitation energies when only the polarization energy is included within the cluster C_2 . The data of the last two columns also contain the field energy from outside the cluster C_2 , which is obtained from Eq. (30) for $n=0$ and 1, respectively.

	$\Delta\epsilon_{\text{SCF}}(\vec{k})$	$\Delta\epsilon(\vec{k}, C_2)$	$\Delta\epsilon^{(n)}(\vec{k})$	
			$n=0$	$n=1$
${}^u\Gamma_1 \rightarrow {}^u\Gamma_{25'}$	29.0	24.6	23.1	23.0
${}^c\Gamma_{15} \rightarrow {}^c\Gamma_2$	11.5	10.1	9.6	9.8
${}^u\Gamma_{25} \rightarrow {}^c\Gamma_{15}$	15.0	9.5	7.0	7.0
${}^uX_4 \rightarrow {}^cX_1$	23.9	17.9	15.0	15.1

the SCF calculation are upward (downward) shifts of the valence (conduction) bands. This results in a reduction of the direct gap from 15.0 to 7.0 eV. The energy corrections are significantly larger for the bottom of the valence band than for the top, leading to a reduction of the valence-band width from 29.0 to 23.1 eV. These trends are in agreement with the arguments resulting from second-order perturbation theory.¹⁷ The closeness of the direct gap and of the valence-band width to the experimental values of 7.3 (Ref. 7) and 24.2 eV, (Ref. 8) respectively, indicates a near cancellation of the changes in the ground-state correlations and the relaxation effects. Both are discussed in more detail in the next section.

We finish this section by a discussion of the physical effects which have led to the energy band changes seen in Fig. 1. The dominant effect is the polarization of the bonds in the neighborhood of the additional electron. The polarization of bond j is described by the difference in the $\eta_{mn}^{(e)}$ parameters

$$\pi_j(\vec{k}, b) = \frac{1}{2} [\eta_{1,2}^{(e)}(0, j) - \eta_{2,1}^{(e)}(0, j)]. \quad (31)$$

Here the first subscript denotes the hybrid in the central bond 0, while the second subscript refers to the hybrid in bond j . According to Eq. (6), the $\eta^{(e)}$ parameters refer to density or charge correlations between these two regions. We found from our calculations that three $\pi_j(\vec{k}, b)$ parameters for each pair of values (\vec{k}, b) are sufficient in order to reproduce about 98% of the correlation energy which is obtained with the set of 14 independent $\eta_{mn}^{(e)}$ parameters. This indicates the small contribution of charge transfer (see Sec. V of I) to the correlation energy of diamond. The three $\pi_j(\vec{k}, b)$ parameters are listed in Table III for the highest valence and lowest conduction band at the points Γ and X . They describe the polarization of the nearest-neighbor and second-nearest-neighbor bond in parallel and nonparallel position. This polarization is shown in Fig. 2. For larger distances the polarization is according to the continuum approximation. It is seen from Table III that the polarization has different signs for the electron and the hole. Furthermore, there is no strict electron-hole symmetry present due to the differences in the conduction and valence bands.

In addition to the bond polarization, there is a further contribution to the total polarization which can be interpreted as a charge transfer. Its main effect is to reduce the charge within the central bond containing the extra

TABLE III. Variation parameters $\pi_j(\vec{k}, b)$ at selected symmetry points characterizing the polarization of the first-neighbor bonds π_1 and of the second-nearest-neighbor bonds parallel π_2^p and nonparallel π_2^{np} .

$\pi_j(\vec{k}, b)$	π_1	π_2^p	π_2^{np}
${}^c\Gamma_{15}$	0.149	0.049	0.041
${}^u\Gamma_{25'}$	-0.112	-0.053	-0.044
uX_4	-0.137	-0.065	-0.051
uL_1	-0.174	-0.088	-0.056

electron by an amount δq . This charge is transferred from bond to bond up to the surface. This resembles to some extent the screening mechanism in metallic systems. It is important to notice that there is no charge transfer if the Wannier functions are chosen within the BOA [see Eq. (23)]. In that case, the charge in a bond is always two. Charge transfer can occur only when the Wannier functions are chosen according to the EBOA [see Eq. (25)]. This has been discussed in detail in I. In order to estimate the size of the charge transfer contribution to the correlation energy, we have performed an independent calculation of the latter. Thereby we have chosen Wannier functions as given by Eq. (23). The corresponding changes in $\epsilon_{\text{corr}}(\vec{k}, b)$ were found to be small. In particular, the direct gap was found to be 7.5 eV instead of 7.0 eV. This corresponds to a reduction of the charge in the central bond by about $0.05e$. That the changes due to the EBOA are small is mainly a consequence of the large gap and the good localization of the Wannier functions in diamond. For Si or Ge we expect the charge transfer to be more important.

This concludes our discussion of the polarization effects. It is seen that the corresponding physical picture is very simple and intuitive. What remains is a discussion of the changes in the ground-state correlations and the relaxation in the neighborhood of the extra electron and hole.

V. GROUND-STATE CORRELATION AND RELAXATION EFFECTS

In the preceding section the polarization caused by an extra electron has been evaluated under two restrictions. Firstly, the calculations were done within a minimal basis set, thus excluding orbital relaxation effects, and secondly, the influence of the ground-state correlations on the correlation energy of the quasiparticle was neglected by putting $\eta_{mn}^{(0)} = 0$ in the respective equations.

Let us start by discussing the effect of the ground-state correlations. As can be seen from Eqs. (17) and (18), their influence on the correlation energy is twofold. They modify the variational parameters $\eta_{mn}^{(e)}(\vec{k}, b)$ through Eq. (17), and they contribute an additional term $\epsilon_{\text{corr}}^{(0)}(\vec{k}, b)$ to $\epsilon_{\text{corr}}(\vec{k}, b)$ [see Eq. (18)]. Physically, the energy change $\epsilon_{\text{corr}}^{(0)}(\vec{k}, b)$ is due to the blocking of two-particle excited states within the central bond in the presence of the extra electron (when a hole is present there is also no correlation energy left in the central bond). Thus $\epsilon_{\text{corr}}^{(0)}(\vec{k}, b)$ has only a weak \vec{k} dependence (see Sec. V of I). Therefore instead of evaluating $\epsilon_{\text{corr}}^{(0)}(\vec{k}, b)$ from Eq. (18) numerically, we identify it with the negative of the interatomic correlation energy within a bond found in Ref. 3 for the ground state of diamond, i.e., $\epsilon_{\text{corr}}^{(0)} = -0.4$ eV. The related variational parameter $\eta_{nn}^{(0)}$ was denoted there by η_1 and was found to be 0.32, implying a reduction of double occupancy within a hybrid by about 16%. This value for $\epsilon_{\text{corr}}^{(0)}$ is used for the extra electron as well as for the hole.

The second effect of the ground-state correlations is to affect Eq. (17). The reduction of double occupancy of the hybrid orbitals in the correlated ground state counteracts the bond polarization and leads to a reduction of the parameters $\eta_{mn}^{(e)}$. The evaluation of Eq. (17) requires matrix

elements of the form $((O_{m'n'}^{(0)})^\dagger HO_{m'n'}^{(e)})_{\vec{k}, \vec{b}}$ as additional input which can be calculated with the help of Eq. (B9) of I. The reduction of the correlation energy $\epsilon^{(e)}(\vec{k}, \vec{b})$ again depends on \vec{k} and \vec{b} and varies between 0.5 and 1.2 eV for the top and bottom of the valence band. The parameters $\eta_{mn}^{(e)}$ are reduced by 10–15%. The band structure containing the ground-state correlation effects is plotted in Fig. 4, where the band structure including only polarization effects is also shown.

Next we consider those contributions to the correlation energy which cannot be described within the minimal basis set. The most important among those is the *relaxation* of the orbitals close to the charge of the quasiparticle. The electron orbitals in the central and nearby bonds contract or expand in the same way as atomic orbitals do when a charge is taken off or added to an atom. This effect can be described within the formalism of I by simply working within a larger basis set. However, the extended basis set is only required for the atoms close to the extra particle and not for the whole cluster. The necessary calculations have not yet been done though. Therefore we use molecular data in order to obtain an estimate for the energy gain by relaxation. For ethane (C_2H_6), which has an electronic structure similar to that of diamond, Moscardo *et al.*¹⁸ performed independent SCF calculations for the ground state and various ionized states of the ion $C_2H_6^+$. By comparing the ionization potentials as obtained from Koopmans's theorem on one side and from the energy differences of the SCF calculations on the other side, one can infer a relaxation energy of 0.76 ± 0.05 eV for the different states of the $C_2H_6^+$ ion. If we assume that the same relaxation occurs for the hole and the electron in diamond, then this leads to a reduction of the

direct gap by 1.5 eV, and therefore to an almost complete compensation of the corrections resulting from the ground-state correlations.

There is another correction which can occur when the basis set is enlarged, namely an increase in the polarizability of the bonds. Until now we have calculated it only within the minimal basis set. Although this will certainly yield the dominant contribution to it, there can be an additional increase when the basis set is enlarged.

However, the resulting change in the correlation energy is small. This is seen by writing the polarization energy W in a continuum approximation in the form

$$W = \frac{1}{2} \int d^3r \vec{P} \cdot \vec{E}_0 \\ = -\frac{1}{2} \frac{\epsilon_0 - 1}{\epsilon_0} \frac{e^2}{r_c} \quad (32)$$

Here \vec{E}_0 is the bare electric field of an electron, i.e., in the absence of the polarization \vec{P} , and r_c is a cutoff which is of the order of a bond length. Let us assume that a larger basis set leads to a change in the dielectric constant ϵ_0 by an amount $\delta\epsilon_0$. Then the resulting change in the polarization energy is

$$\frac{\delta W}{W} = \frac{1}{\epsilon_0 - 1} \frac{\delta\epsilon_0}{\epsilon_0} \quad (33)$$

and therefore considerably smaller than $\delta\epsilon_0/\epsilon_0$. For that reason we can neglect it here.

In Table IV we list the energy shifts at selected symmetry points as obtained without taking ground-state correlation effects into account [LA(1)], with inclusion of these effects [LA(2)] and including also the estimated relaxation effects [LA(3)]. Also shown for comparison are the results of the screened-exchange-plus-Coulomb-hole approach (SECH) as obtained by Brener¹⁹ and these of the time-dependent screened Hartree-Fock (TDSHF) or Green's-function approach.^{16,20}

The general trend of our results is in agreement with those of the two other approaches, with the SECH somewhat better than with the TDSHF. As far as the SECH is

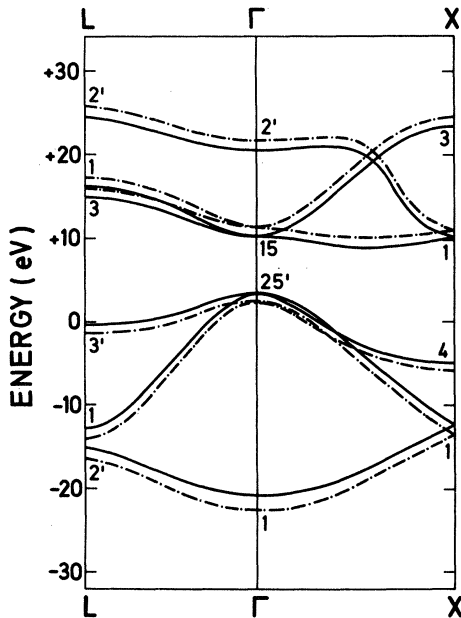


FIG. 4. Quasiparticle bands as obtained by taking ground-state correlation effects into account LA(2) (dashed-dotted lines). For comparison, the bands are shown which include polarization effects [LA(1)] only (solid lines).

TABLE IV. Comparison of the correlation energy corrections to the SCF energies at typical symmetry points in units of eV. Columns LA(1) through LA(3) give results of this work, LA(1) includes polarization only, LA(2) contains, in addition, the effect due to the ground-state correlation, and LA(3) contains estimated corrections resulting from orbital relaxation as well.

	SECH ^a	TDSHF ^b	LA(1)	LA(2)	LA(3)
^c $\Gamma_{2'}$	5.0	4.1	6.5	5.3	6.0
^c Γ_{15}	3.6	3.4	4.5	3.6	4.3
^c $\Gamma_{25'}$	2.5	4.1	3.5	2.6	3.3
^e Γ_1	5.5	8.4	9.4	7.9	8.5
^e X_1	4.2	3.1	4.6	3.6	4.3
^e X_4	3.7	5.3	4.2	3.3	4.0

^aFrom Ref. 19.

^bFrom Ref. 16.

concerned, our values are significantly larger for large quasiparticle energies, e.g., at the bottom of the valence band. This can be argued to result from the neglect of the frequency dependence of the dielectric function in the SECH approach. Also the reduction of the valence-band width is only 3.1 eV in that approach, as compared with 5.9 eV in the LA(1) calculation. In the TDSHF calculation, a slightly larger energy change is found at the top of the valence band then for the bottom of the conduction band. This is contrary to our findings and those in the SECH approach. In our treatment the slightly larger correction for the bottom of the conduction band results from the fact that the conduction band is narrower than the valence band.

In Table V a comparison is given for the results of the direct gap and the valence-band width as obtained by the different approaches including the density-functional method in its local approximation (LDA). As mentioned before we find that a minimal basis set is not sufficient in order to produce energy bands with an accuracy of a few tenths of an electron volt, i.e., that relaxation effects are important. This contrasts the findings of Refs. 16 and 20. A more detailed comparison with the LDA and the TDSHF approach is found in the next section.

VI. COMPARISON WITH OTHER METHODS

In the following we want to compare the physical picture which has emerged from the above correlation energy treatment with that of alternative methods. Of those we want to consider in particular the LDA. As is well known, this method is by far the simplest and most efficient method for calculating energy bands in solids. In particular, its application to semiconductors shows that it does not have the shortcomings of the SCF calculations which lead to too large energy gaps. On the contrary, in most cases the energy gap is found to be smaller in the LDA than the experimental one. In particular, this holds true for diamond, where all-electron local-density-functional calculations²¹ yield a direct energy gap of 5.55 eV when the linear combination of muffin-tin orbitals method is used within the atomic sphere approximation. The larger value of 6.3 eV (Ref. 22) found within the linear combination of atomic orbitals scheme may be

caused by the highly anomalous dispersion of the conduction band in the Δ direction close to the cX_1 point.

It is instructive to analyze the source of the reduction of the SCF energy gap in that case. When one does a SCF calculation with the *nonlocal* exchange replaced by a *local* exchange potential, one finds for diamond an energy gap which comes close to the experimental one, i.e., of the order of 6–7 eV.²³ It is, therefore, much smaller than that which results when a nonlocal exchange is used. Additional inclusions of correlations, i.e., replacing the local exchange potential by a local exchange-correlation potential, do not change the value of the energy gap appreciably. The LDA calculations are, therefore, relatively insensitive to the inclusion of correlation effects in distinction to the present investigation. One can, of course, argue that it is the compensation of errors in the local approximation to the exchange and correlation potentials which makes the LDA such a successful scheme, and that it is therefore unjustified to use a local approximation for the exchange only when performing a SCF calculation. For that reason it is instructive to consider the exchange-correlation potential $\mu_{xc}(\vec{r})$ from a different point of view which is from Gunnarsson and Lundqvist.²⁴ It is

$$\mu_{xc}(\vec{r}) = \frac{\delta}{\delta\rho(\vec{r})} \frac{1}{2} \int d^3r' d^3r'' \frac{\rho(\vec{r})\rho_{xc}(\vec{r}, \vec{r}-\vec{r}')}{|\vec{r}-\vec{r}'|}, \quad (34)$$

$$\rho_{xc}(\vec{r}, \vec{r}-\vec{r}') = \rho(\vec{r}') \int_0^1 d\lambda [g(\vec{r}, \vec{r}'; \lambda) - 1].$$

Here $\rho(\vec{r})$ is the density and $\rho_{xc}(\vec{r}, \vec{r}-\vec{r}')$ is a fictitious exchange-correlation hole charge of an electron at position \vec{r} . The function $\rho_{xc}(\vec{r}, \vec{r}-\vec{r}')$ is related to the pair distribution function $g(\vec{r}, \vec{r}', \lambda)$, where λ denotes the coupling constant. Furthermore, $\rho_{xc}(\vec{r}-\vec{r}')$ satisfies the sum rule

$$\int d^3r' \rho_{xc}(\vec{r}, \vec{r}') = -1. \quad (35)$$

In the LDA, $g(\vec{r}, \vec{r}', \lambda)$ is replaced by that of a homogeneous electron gas $g_h(\vec{r}-\vec{r}'; \lambda; \rho(\vec{r}))$ and furthermore $\rho(\vec{r}')$ by $\rho(\vec{r})$.

For diamond $g_h(\vec{r}-\vec{r}')$ appears qualitatively as shown in Fig. 5(a). In distinction to this the exchange-correlation hole around an additional electron in the conduction band appears as shown in Fig. 5(b), and around an electron in a

TABLE V. Comparison of the experimental direct band gap and the valence-band width with results from various calculations in units of eV. The results of this work LA(1)–LA(3) are as defined in Table IV.

	Expt.	HF ^c	LDA ^d	TDSHF ^e	LA(1)	LA(2)	LA(3)
${}^u\Gamma_{25'} \rightarrow {}^c\Gamma_{15}$	7.3 ^a	15.0	5.5	7.4	7.0	8.8	7.4
${}^u\Gamma_1 \rightarrow {}^u\Gamma_{25'}$	24.2 ^b	29.0	21.3	25.2	23.1	23.7	23.8
${}^uX_4 \rightarrow {}^cX_1$	12.5 ^a	23.9	10.5	15.9	15.1	17.0	15.6

^aFrom Ref. 7.

^bFrom Ref. 8.

^cFrom Ref. 4.

^dFrom Ref. 21.

^eFrom Ref. 16.

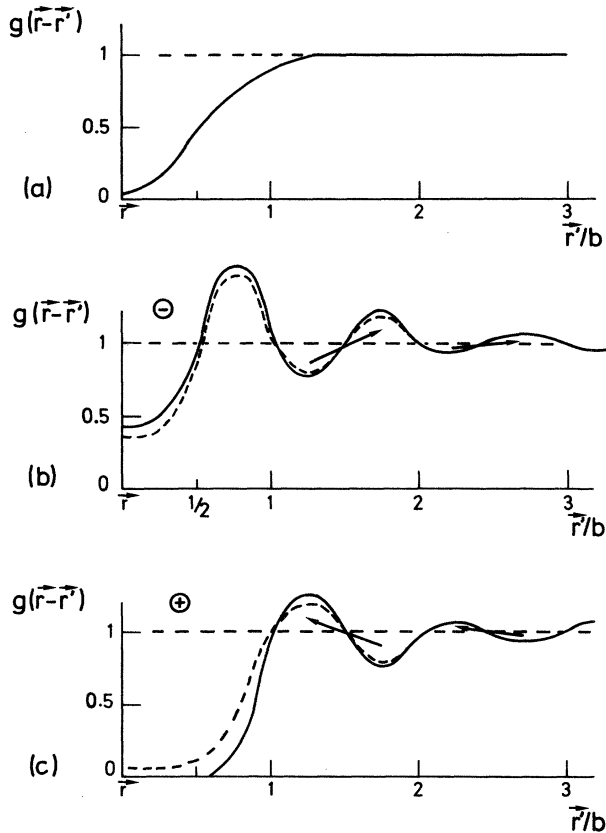


FIG. 5. Schematic comparison of the pair correlation function $g(\vec{r}-\vec{r}')$ for (a) the homogeneous electron gas and for an electron in diamond sitting in a bond together with (b) an extra electron or (c) a hole. The oscillatory behavior of $g(\vec{r}-\vec{r}')$ for (b) and (c) indicates the polarization cloud decaying proportional to $|\vec{r}-\vec{r}'|^{-2}$. The dashed line indicates the changes resulting from charge transfer. Here the vector $\vec{r}-\vec{r}'$ follows a bond sequence, and b is the bond length.

bond containing a hole as indicated in Fig. 5(c). It has been shown in Sec. IV that for diamond the charge transfer to the surface is only 0.05 of an electron charge when an electron is added. Therefore integration over $[g(\vec{r},\vec{r}')-1]$ yields almost zero in Fig. 5(b) and almost -2 in Fig. 5(c). Assuming that the charge transfer increases up to the metallic case, then the integration would yield -1 in the electron and hole case as in Fig. 5(a). The oscillations in Figs. 5(b) and 5(c) fall off proportionally to r^{-2} and result from the bond polarizations. It is apparent that no polarization effect proportional to r^{-2} is present in the LDA which is based on the homogeneous electron gas. It is that part of the pair distribution function which leads to the reduction of the SCF direct energy gap, while the part within the first bond is responsible for the changes in the ground-state correlations. It should be mentioned that in the *ground* state of diamond the pair distribution function looks different than Figs. 5(b) and 5(c). In that case one has a van der Waals interaction between electrons in different bonds, and the oscillations fall off as r^{-6} . Then the pair distribution function resembles more closely that of Fig. 5(a). The LDA cannot distin-

guish between the two different situations in the ground state and excited state. Since the overall density is the same in both cases, so is $\mu_{xc}(\vec{r})$ and therefore the exchange-correlation energy contribution. From the above we expect that the LDA is better the more delocalized the Wannier functions are.

We can analyze the results contained in Fig. 4 in terms of an energy-dependent correlation potential. For that purpose we select a number of points in \vec{k} space and plot, in Fig. 6 for each point, the correlation energy as a function of the energy $\epsilon(\vec{k},b)$. It is of considerable interest to see that the correlation energy may be fairly well approximated by a functional of the energy, and that matrix element effects¹⁷ seem to be of minor importance. However, the ϵ_{corr} vs ϵ curve for the conduction bands is flatter than that for the valence bands, which implies that the conduction-band width is reduced less. This particular feature may be considered as a matrix element effect, but it is small. This suggests the introduction of a local but energy-dependent correlation potential into the single-particle Schrödinger equation. There have been attempts before defining such potentials.²⁵⁻²⁷ From the foregoing, at least for diamond, a potential of the form $V_{\text{corr}}(\epsilon) = a + b\epsilon^2$ seems to be well justified with $a=4$ eV and $b=7.5 \times 10^{-3}$ eV⁻¹. As discussed before, this requires the inclusion of nonlocal exchange effects in the density-functional scheme.

Next, we want to compare the present approach with the Green's-function approach, which employs the dielectric response theory.^{16,20} This approach also uses a minimal basis set consisting of four valence and conduction bands, respectively. A comparison of the energy corrections for the top and bottom of the conduction and valence bands is shown in Table IV. The corresponding excitation energies can be read from Table V. An important difference in our results is that whereas we believe to have proved that a reduction of the direct gap to the experimental value requires the inclusion of relaxation ef-

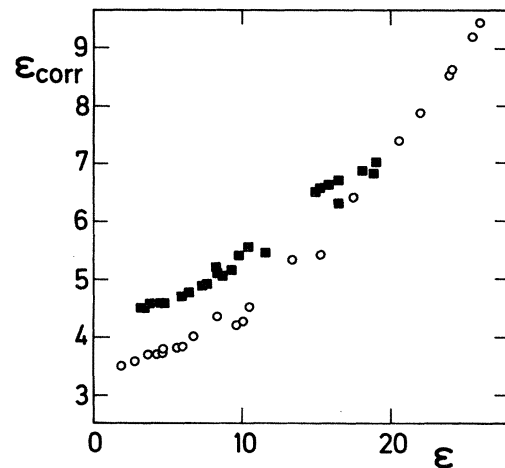


FIG. 6. Plot of the correlation energy $\epsilon_{\text{corr}}(\vec{k},b)$ vs the total energy $\epsilon(\vec{k},b)$ for valence bands (circles) and conduction bands (squares) in units of eV. The different points correspond to different values of (\vec{k},b) .

fects, such a reduction is obtained in Refs. 16 and 20 even within the minimal basis set. The reason for this discrepancy is probably due to the fact that the calculations of Refs. 16 and 20 contain a phenomenologically introduced screening of the exchange. This is something which cannot be described within a minimal basis set and might have the effect of simulating relaxation effects.

Another assumption of Refs. 16 and 20 is proven valid by our calculations. This concerns restricting oneself to bubble and exchange ladder diagrams. We find within our variational approach that the diagrams 3(a)–3(d) of Fig. 6 in I are by far the most important of those which are second order in $\eta^{(e)}$. From our experience with small molecules we expect that this is different for intra-atomic correlations where all diagrams of Fig. 6 should become equally important. A more detailed comparison between the two approaches is not possible because the calculations in Refs. 16 and 20 are done in q space. Therefore we cannot check how large the important polarizations of the bonds close to the added electrons come out to be in that approach. It is the accurate determination of these polarizations which we consider to be an advantage of our approach.

VII. SUMMARY AND CONCLUSIONS

It has been shown by means of a local approach to the correlation problem that the correlation energy can be calculated for excited states of diamond. The correlation energy results mainly from a polarization of the neighborhood of the electron in the conduction band and the hole in the valence band. The present approach allows for an accurate calculation of that polarization in the nearest-neighbor and next-nearest-neighbor bonds. Beyond these, a continuum approximation has been used in order to reduce the computational effort. In addition to the polarization effects the reduction of the ground-state correlations due to the excitation was found to be important. Relaxation effects have only been estimated here, although they are contained in the general formalism. Once the local expectation values (13) were calculated the energy-band calculations themselves required approximately 1 min of processor time on a HB-DPS 66 machine.

Futural extensions of the present approach will concern the inclusion of relaxation effects and an extension to other semiconducting systems. Also, it appears to be of interest to incorporate into the present theory excitonic excitations. We believe that the present approach is able to attach a simple physical picture to the various correlation energy contributions because it is local in character. It can be used to achieve an accuracy which is comparable to that of the coupled-pair approximation (CEPA) in quantum chemistry for small molecules. The computational bottleneck seem to be the SCF calculations which are required as the starting point. Although for diamond there are SCF calculations available of high quality the estimated uncertainties in the energy bands are still of the order of 1 eV. From that point of view it appears as a challenging problem for the future to see whether the SCF part of the calculations can be substantially improved and simplified.

ACKNOWLEDGMENTS

We would like to thank Dr. G. Stollhoff for many helpful discussions and remarks and Dr. B. Kiel for making available his Hartree-Fock program to us. We also gratefully acknowledge interesting conversations with Dr. O. Gunnarsson and Dr. W. Hanke.

APPENDIX: EVALUATION OF THE MATRICES (14) IN THE CASE OF INTERATOMIC CORRELATIONS

In the following, detailed information required for the evaluation of the matrices (14) is provided in the case where the Hamiltonian and the correlation operators O_{mn} are defined in terms of the minimal basis sets $\tilde{f}_i(\vec{r})$ (21) and $g_m(\vec{r})$ (26), respectively. By using the definition (26) of the functions $g_m(\vec{r})$ the corresponding operators $b_{m\sigma}^\dagger$ can be expressed in terms of operators $w_{i\sigma}^\dagger$ which generate electrons in Wannier states as defined by Eq. (25) as

$$b_{n\sigma}^\dagger = \sum_{\underline{l}, \tau=1}^4 \alpha_{n\tau} w_{i\sigma}^\dagger + \sum_{\underline{l}, \tau=5}^8 \beta_{n\tau} w_{i\sigma}^\dagger. \quad (\text{A1})$$

The expansion coefficients $\alpha_{n\tau}$ and $\beta_{n\tau}$ are obtained from (26) and by inversion of (25).

Because of the orthogonality relations $\langle w_{i\sigma}^\dagger w_{i'\sigma'} \rangle = \delta_{\sigma\sigma'} \delta_{ii'}$ ($\tau=5, \dots, 8$) and zero otherwise, one obtains

$$\bar{P}_{mn} = \langle b_{m\sigma}^\dagger b_{n\sigma} \rangle = \sum_{\underline{l}, \tau=5}^8 \beta_{m\tau} \beta_{n\tau}, \quad (\text{A2})$$

and from the orthogonality of the $g_n(\vec{r})$, $\bar{D}_{mn} = \delta_{mn} - \bar{P}_{mn}$. Since we are working with the basis set described by the $\tilde{a}_{i\sigma}^\dagger$ and $\tilde{a}_{i\sigma}$ operators, the matrices in (14) are also defined with respect to the latter, i.e., $R_{im} = \langle \tilde{a}_{i\sigma}^\dagger b_{m\sigma} \rangle$, etc. It is convenient to relate all these matrices to the density matrix $\langle a_{i\sigma}^\dagger a_{j\sigma} \rangle$. We can divide the latter into a part resulting from the core electrons $\langle a_{i\sigma}^\dagger a_{j\sigma} \rangle_{\text{core}}$ and a part due to the occupied valence bands. By making use of Eqs. (7) and (A2), one can show that

$$\langle a_{i\sigma}^\dagger a_{j\sigma} \rangle = \sum_{m,n} \gamma_{mi} \gamma_{nj} \bar{P}_{mn} + \langle a_{i\sigma}^\dagger a_{j\sigma} \rangle_{\text{core}}. \quad (\text{A3})$$

The core contribution to the density matrix is of no relevance as long as one is interested in matrices which contain at least one operator $b_{n\sigma}$ or $w_{i\sigma}$.

The $\tilde{a}_{i\sigma}^\dagger$ operators are related to the $a_{j\sigma}^\dagger$ through Eq. (21),

$$\tilde{a}_{n\sigma}^\dagger = \sum_i \tilde{c}_{ni} a_{i\sigma}^\dagger, \quad \tilde{c}_{ni} = \sum_{m,j} \tilde{S}_{nm}^{-1} c_{mj} S_{ji}. \quad (\text{A4})$$

Thereby the overlap matrix $\langle \tilde{f}_i | \tilde{f}_j \rangle = \tilde{S}_{ij}$ has been defined in analogy to the matrix S_{ij} . Similarly, the $b_{m\sigma}^\dagger$ are expressed in terms of the $a_{i\sigma}^\dagger$ by making use of Eq. (7):

$$b_{m\sigma}^\dagger = \sum_{i,j} \gamma_{mj} S_{ji} a_{i\sigma}^\dagger. \quad (\text{A5})$$

With these relations one obtains

$$R_{mn} = \langle \tilde{a}_{m\sigma}^\dagger b_{n\sigma} \rangle = \sum_{i,s} \tilde{c}_{mi} \gamma_{si} \bar{P}_{sn}, \quad (\text{A6})$$

$$D_{mn} = \langle \tilde{a}_{m\sigma}^\dagger b_{n\sigma}^\dagger \rangle = \sum_{i,s} \tilde{c}_{mi} \gamma_{si} \bar{D}_{sn},$$

where use has been made of the orthogonality of the $g_n(\vec{r})$ from which it follows that $\sum_{i,j} \gamma_{mi} \gamma_{nj} S_{ij} = \delta_{mn}$.

The remaining matrices are written with the help of (A1) as

$$\bar{C}_{mt} = \langle b_{m\alpha} w_{t\sigma}^\dagger \rangle = \begin{cases} \alpha_{mt}, & \tau=1, \dots, 4 \\ 0, & \tau=5, \dots, 8 \end{cases} \quad (\text{A7})$$

$$C_{mt} = \langle a_{m\sigma} w_{t\sigma}^\dagger \rangle = \begin{cases} \sum_n \alpha_{nt} D_{mn}, & \tau=1, \dots, 4 \\ 0, & \tau=5, \dots, 8. \end{cases} \quad (\text{A8})$$

Knowing those matrices and the $\tilde{\epsilon}_{ij}$ and \tilde{V}_{ijkl} one can evaluate the expectation values (13) according to the rules given in I.

- ¹S. Horsch, P. Horsch, and P. Fulde, *Phys. Rev. B* **28**, 5977 (1983).
- ²G. Stollhoff and P. Fulde, *J. Chem. Phys.* **73**, 4548 (1980).
- ³B. Kiel, G. Stollhoff, C. Weigel, P. Fulde, and H. Stoll, *Z. Phys. B* **46**, 1 (1982); see also B. Kiel, G. Stollhoff, P. Fulde, and H. Stoll, *Phys. Lett.* **87A**, 433 (1982).
- ⁴A. Mauger and M. Lannoo, *Phys. Rev. B* **15**, 2324 (1977).
- ⁵R. N. Euwema, D. L. Wilhite, and G. T. Surratt, *Phys. Rev. B* **7**, 818 (1973).
- ⁶R. Dovesi, C. Pisani, F. Ricca, and C. Roetti, *Phys. Rev. B* **22**, 5936 (1980).
- ⁷R. A. Roberts and W. C. Walker, *Phys. Rev.* **161**, 730 (1967).
- ⁸F. R. McFeely, S. R. Kowalczyk, L. Ley, R. G. Cavell, R. A. Pollak, and D. A. Shirley, *Phys. Rev. B* **9**, 5268 (1974). Recent ultraviolet photoelectron spectroscopy (UPS) measurements by F. J. Himpsel, J. F. van der Veen, and D. E. Eastman [*Phys. Rev. B* **22**, 1967 (1980)] give a valence-band width of 21.0 ± 1 eV. It could be that surface effects are responsible for this lower value, but it has also been argued that the UPS data are more consistent with other measurements.
- ⁹J. C. Slater and G. F. Koster, *Phys. Rev.* **94**, 1498 (1954).
- ¹⁰H. Stoll and H. Preuss, *Int. J. Quantum Chem.* **9**, 775 (1975).
- ¹¹H. Stoll, G. Wagenblast, and H. Preuss, *Theor. Chim. Acta* **57**, 169 (1980).
- ¹²B. Roos and P. Siegbahn, *Theor. Chim. Acta* **17**, 209 (1970).
- ¹³In Ref. 3, instead of the $f_n(\vec{r})$, functions $f_n^\mu(\vec{r})$ were introduced with μ being a site (not cell) index, while n labels the 12 basis functions per atom.
- ¹⁴P.-O. Löwdin, *J. Chem. Phys.* **18**, 365 (1950).
- ¹⁵W. A. Harrison, *Electronic Structure and the Properties of Solids* (Freeman, San Francisco, 1980).
- ¹⁶G. Strinati, H. J. Mattausch, and W. Hanke, *Phys. Rev. B* **25**, 2867 (1982).
- ¹⁷S. T. Pantelides, D. J. Mikish, and A. B. Kunz, *Phys. Rev. B* **10**, 2602 (1974).
- ¹⁸F. Moscardó, M. Paniagua, and E. San-Fabian, *Theor. Chim. Acta* **54**, 53 (1979).
- ¹⁹N. E. Brener, *Phys. Rev. B* **11**, 929 (1975).
- ²⁰W. Hanke and L. Sham, *Phys. Rev. Lett.* **33**, 582 (1974); see also W. Hanke, *Adv. Phys.* **27**, 287 (1978).
- ²¹D. Glötzel, B. Segall, and O. K. Andersen, *Solid State Commun.* **36**, 403 (1980).
- ²²A. Zunger and A. J. Freeman, *Phys. Rev. B* **15**, 5049 (1977).
- ²³K.-P. Bohnen (private communication).
- ²⁴O. Gunnarsson and B. I. Lundqvist, *Phys. Rev. B* **13**, 4274 (1976).
- ²⁵L. J. Sham and W. Kohn, *Phys. Rev.* **145**, 561 (1966).
- ²⁶U. von Barth and L. Hedin, *Nuovo Cimento* **23B**, 1 (1974).
- ²⁷W. Hanke (private communication).